Geophysical Research Letters®

Distribution and Trend of Wind Power Input to Near-Inertial Motions in the Southern Ocean

Jiangchao Qian[1,2], Xiaoming Zhai[3] ![ORCID], Zhaomin Wang[4], and Markus Jochum[5]

[1]Key Laboratory of Marine Hazards Forecasting, Ministry of Natural Resources, Hohai University, Nanjing, China, [2]College of Oceanography, Hohai University, Nanjing, China, [3]Centre for Ocean and Atmospheric Sciences, School of Environmental Sciences, University of East Anglia, Norwich, UK, [4]Southern Marine Science and Engineering Guangdong Laboratory (Zhuhai), Zhuhai, China, [5]Physics of Ice, Climate and Earth, Niels Bohr Institute, University of Copenhagen, Copenhagen, Denmark

Abstract Wind power input to near-inertial motions is an important energy source for generating diapycnal mixing in the ocean. However, the distribution and long-term trend of this input over the Southern Ocean have yet to be quantified. In this study, we investigate the near-inertial wind power input (WPI_i) to the Southern Ocean using a global eddy-permitting coupled ocean-sea ice model forced by a high-resolution atmospheric reanalysis product. Our results reveal a zonally asymmetric distribution of WPI_i in the Southern Ocean, with the strongest input in the South Indian Ocean and the weakest in the South Pacific. The integrated WPI_i between 30°S and 60°S exhibits a significant positive trend over the past four decades due to the intensification of mesoscale weather systems. The surface mixed-layer depth is found to modulate the spatial pattern and trend of WPI_i by altering the surface near-inertial currents.

Plain Language Summary Wind fluctuations can excite surface ocean currents that oscillate at frequencies close to the inertial frequency. These near-inertial motions play an important role in generating turbulent mixing in the ocean. However, the distribution and long-term trend of wind power input to near-inertial motions in the Southern Ocean remains unquantified. In this study, we investigate this wind power input using a global ocean circulation model driven by a high-resolution atmospheric reanalysis data set. Our results reveal a pronounced zonal asymmetry in the distribution of near-inertial wind power input in the Southern Ocean. Furthermore, this power input has increased significantly over the past four decades due to the intensification of mesoscale weather systems. Results from this study have important implications for understanding Southern Ocean mixing and circulation.

1. Introduction

Near-inertial motions dominate the internal-wave spectrum of the ocean (Kunze, 1985). They are predominantly excited by fluctuating winds and are an important energy source for generating diapycnal mixing in the upper and deep ocean, contributing to the cooling of the sea surface (e.g., Jochum et al., 2013) and the maintenance of the large-scale overturning circulation (Wunsch & Ferrari, 2004). The wind power input to near-inertial motions (WPI_i) has often been estimated using a combination of various wind stress products and simplified ocean dynamics such as slab ocean models. The global-integrated values of WPI_i range from 0.29 to 1.40 TW, depending on the wind products used (Alford, 2001, 2003; Jiang et al., 2005; Rimac et al., 2013; Watanabe & Hibiya, 2002). However, it is known that the slab models do not reproduce the observed kinetic energy balance during strong wind forcing events and they tend to overestimate WPI_i considerably due to the lack of a dissipation mechanism that operates on short time scales (Plueddemann & Farrar, 2006). Ocean general circulation models (OGCM; Furuichi et al., 2008; Simmons & Alford, 2012; Rimac et al., 2013; Flexas et al., 2019) tend to provide more realistic representations of near-inertial energy budget compared to slab models (Flexas et al., 2019). However, due to the large amount of high-frequency model output required for filtering near-inertial currents, studies investigating near-inertial wind power input based on OGCMs are often limited to relatively short periods, typically ranging from a few months to one year (e.g., Dippe et al., 2015; Flexas et al., 2019; Rath et al., 2014). While WPI_i can also be estimated from observations such as ocean currents derived from near-surface drifters (Liu et al., 2019), the lack of long-term drifter data and the uneven distribution of near-surface drifters make it impossible to assess the long-term variability and trend of WPI_i.

The majority of wind power input to near-inertial motions in the ocean is accounted for by winter storm activities at mid-latitudes (e.g., D'Asaro, 1985). These midlatitude winter storms encompass a combination of transient atmospheric phenomena, including synoptic weather systems, cold/warm fronts, and traveling lows that cover a wide range of spatial scales and they provide the bulk of near-inertial wind energy input to the ocean (Alford, 2003; Dippe et al., 2015; Zhai, 2017). Recent studies indicate a poleward shift and intensification of the mid-latitude storm track in the Southern Hemisphere over the past decades (e.g., Chang et al., 2012; Chemke et al., 2022). Additionally, the high latitudes in the Southern Hemisphere are also rich in mesoscale weather systems such as polar lows which tend to form in regions where cold air masses interact with sharp sea surface temperature gradients (Rasmussen & Turner, 2003). Satellite-based observations (e.g., Irving et al., 2010) have reported strong positive trends in the frequency of mesoscale activities over the Amundsen and Bellingshausen Seas during 1999–2008. However, the impact of these changes of storm activities on WPI_i is yet to be investigated.

In this study, we examine the spatial pattern and long-term trend of WPI_i in the Southern Ocean over the past four decades. To do this, we analyze hourly model output from a global eddy-permitting OGCM forced by a state-of-the-art atmospheric reanalysis product. Factors that influence the distribution and trend of WPI_i in the Southern Ocean are also assessed and discussed.

2. Data and Methods

The model used in this study is the MIT general circulation model (MITgcm; Marshall, Adcroft, et al., 1997; Marshall, Hill, et al., 1997) run on the same grid and using some of the same parameters as the Estimating the Circulation and Climate of the Ocean, Phase 2 (ECCO2), which is a high-resolution global ocean and sea-ice data synthesis (Menemenlis et al., 2005). The model employs a cube-sphere grid projection, which permits relatively even grid spacing throughout the entire domain and avoids polar singularities (Adcroft et al., 2004). The mean horizontal grid spacing of the model is roughly 18 km, that is, eddy-permitting in the Southern Ocean. There are 50 vertical levels with varying thickness, ranging from 10 m near the surface to 450 m near the ocean bottom. The subgrid-scale vertical mixing processes are parameterized using the K-profile parameterization (Large et al., 1994), and no explicit eddy parameterization schemes are used in the model. The model is forced by hourly ERA5 atmospheric reanalysis data (Copernicus Climate Change Service (C3S), 2017), obtained from the European Center for Medium-Range Weather Forecasts (ECMWF) for the period from 1979 to 2019 (without data assimilation). The ERA5 atmospheric reanalysis data have a horizontal resolution of approximately 30 km and include variables such as hourly net longwave radiation, net shortwave radiation, humidity, 2-m air temperature, precipitation, and 10-m wind velocity. Monthly mean outputs of surface mixed-layer depth and hourly-mean outputs of wind stress and ocean surface currents for the entire 41-year study period are analyzed here.

The stress (τ) exerted on the ocean is a combination of air-ocean stress (τ_{AO}) and ice-ocean stress (τ_{IO}), and it is calculated using the quadratic drag law:

$$\tau = (1 - \alpha)\tau_{\text{AO}} + \alpha\tau_{\text{IO}}, \tag{1}$$

where

$$\tau_{\text{AO}} = \rho_{\text{air}} C_{\text{ao}} |u_{\text{10m}} - u_{\text{o}}|(u_{\text{10m}} - u_{\text{o}}), \tag{2}$$

$$\tau_{\text{IO}} = \rho_{\text{w}} C_{\text{io}} |u_{\text{ice}} - u_{\text{o}}|(u_{\text{ice}} - u_{\text{o}}). \tag{3}$$

here α is the sea ice concentration, $\rho_{\text{air}} = 1.2 \text{ kg/m}^3$ and $\rho_{\text{w}} = 1{,}027.5 \text{ kg/m}^3$ are the surface air and seawater densities, respectively, C_{ao} is the drag coefficient between air and ocean which is a function of wind speed (Large & Pond, 1981), $C_{io} = 0.0055$ is the drag coefficient between ice and ocean (McPhee, 1980), and u_{10m}, u_{o}, and u_{ice} are the 10-m wind, ocean surface current velocity, and sea ice drift velocity, respectively. Note that it is important to account for relative motions in the wind stress calculation, also known as the relative wind stress effect. This effect can lead to a notable reduction in WPI_i, with a decrease of over 20% in the Southern Ocean (Rath et al., 2013; see also Zhai, 2017).

Following Flexas et al. (2019), we use a fifth-order Butterworth filter to isolate near-inertial currents in the frequency band of [$0.8f/2\pi$, $1.2f/2\pi$], where f is the local inertial frequency. The same filter is also used to extract the near-inertial components of wind stress. The near-inertial wind stress magnitude (NIWSM) is defined as

the magnitude of the near-inertial components of wind stress which is known to be most efficient in exciting near-inertial currents via inertial resonance (e.g., D'Asaro, 1985; Crawford & Large, 1996; Zhai, 2015), that is,

$$\text{NIWSM} = \sqrt{\tau_{x,i}^2 + \tau_{y,i}^2} \tag{4}$$

where $\tau_{x,i}$ and $\tau_{y,i}$ are the band-pass-filtered near-inertial components of surface wind stress. The wind power input to near-inertial motions is estimated as the dot product of surface wind stress and ocean surface near-inertial currents:

$$\text{WPI}_i = \tau \cdot u_i \tag{5}$$

where u_i is the ocean surface near-inertial current velocity.

The mixed-layer depth (MLD), H, in the ECCO2 state estimate is defined as the depth at which the density differs from that at the surface by an equivalent amount to a temperature difference of 0.8°C, an optimal value suggested by Kara et al. (2000). The modeled annual-mean mixed-layer depth is broadly consistent with the observational estimate by Holte et al. (2017) based on Argo profiles, although it should be acknowledged that some unrealistically deep convection occurs at very high southern latitudes in the model simulation, mainly in the Weddell Sea and Ross Sea. Because of that, in this study we focus on the Southern Ocean between 60°S and 30°S.

To investigate the atmospheric conditions associated with near-inertial wind forcing, we analyze the kinetic energy of synoptic and mesoscale weather systems over the past four decades. For synoptic weather systems, threshold time scales of 2 and 8 days are chosen, as atmospheric variability (e.g., wind and air temperature) on time scales of 2–8 days is generally thought to be associated with synoptic weather systems and baroclinic storm activities (e.g., Lin et al., 2018; Yin, 2005). The time scale definitions for mesoscale weather systems vary among previous studies, for example, 1–4 days used in Uotila et al. (2009), 24–48 hr in Pezza et al. (2016), and 6–36 hr in Verezemskaya et al. (2017). To distinguish mesoscale weather systems from their synoptic-scale counterparts (2–8 days), we consider atmospheric systems with characteristic time scales shorter than 2 days as mesoscale systems. Here we apply a 2-day running mean and a 2–8-day fifth-order Butterworth bandpass filter to the original hourly reanalysis winds to filter out wind fluctuations that last less than 2 days (mesoscale) and those within 2–8 days (synoptic), respectively, following the method of Lin et al. (2018).

3. Results

3.1. Spatial Pattern

The distribution of NIWSM averaged over the 41-year study period exhibits a band of large-magnitude values that is elongated in the zonal direction between 60°S and 30°S (Figure 1a). Large values of NIWSM are concentrated to the south of the Indian Ocean and Australia, while low values of NIWSM are generally found in the South Pacific as well as the western part of the South Atlantic. This spatial pattern broadly resembles the intensity distribution of mesoscale weather systems (Figure S1 in Supporting Information S1). The average value of NIWSM in the Indian Ocean and south of Australia (20°–140°E) is about 0.023 N/m², while that in the South Pacific and western part of the South Atlantic (180°–30°W) is 0.018 N/m². Consistent with the findings of Rath et al. (2014), the maximum values of NIWSM are shifted equatorward compared to those of the total wind stress (Figure S1 in Supporting Information S1). This shift can be explained by the longer inertial periods at lower latitudes which effectively sample greater wind stress variability (Dippe et al., 2015; Zhai, 2015).

The surface near-inertial currents, on the other hand, display a very different spatial pattern (Figure 1b). Apart from one localized area of strong near-inertial currents, the magnitude of near-inertial currents in the Indian Ocean sector and south of Australia tends to be relatively modest. Large values of near-inertial current speed are mostly concentrated in the South Atlantic region. This spatial pattern is broadly consistent with that derived from satellite-tracked near-surface drifter observations during 1999–2006 (Chaigneau et al., 2008), albeit the magnitude of near-inertial currents in our model simulation is on average lower compared to the drifters which may be attributed to insufficient atmospheric forcing and limitations in ocean model resolution (Flexas et al., 2019). Large magnitudes of near-inertial currents are also observed at around 30°S, where the inertial frequency coincides with the diurnal frequency (Dippe et al., 2015; Elipot & Lumpkin, 2008).

The marked difference in the spatial patterns of NIWSM and surface near-inertial currents can be qualitatively understood by considering the solution of the slab model, that is, $|u_i| \propto |\tau_i|/H$, which states that the magnitude of near-inertial currents in the surface mixed layer is proportional to the magnitude of NIWSM and inversely
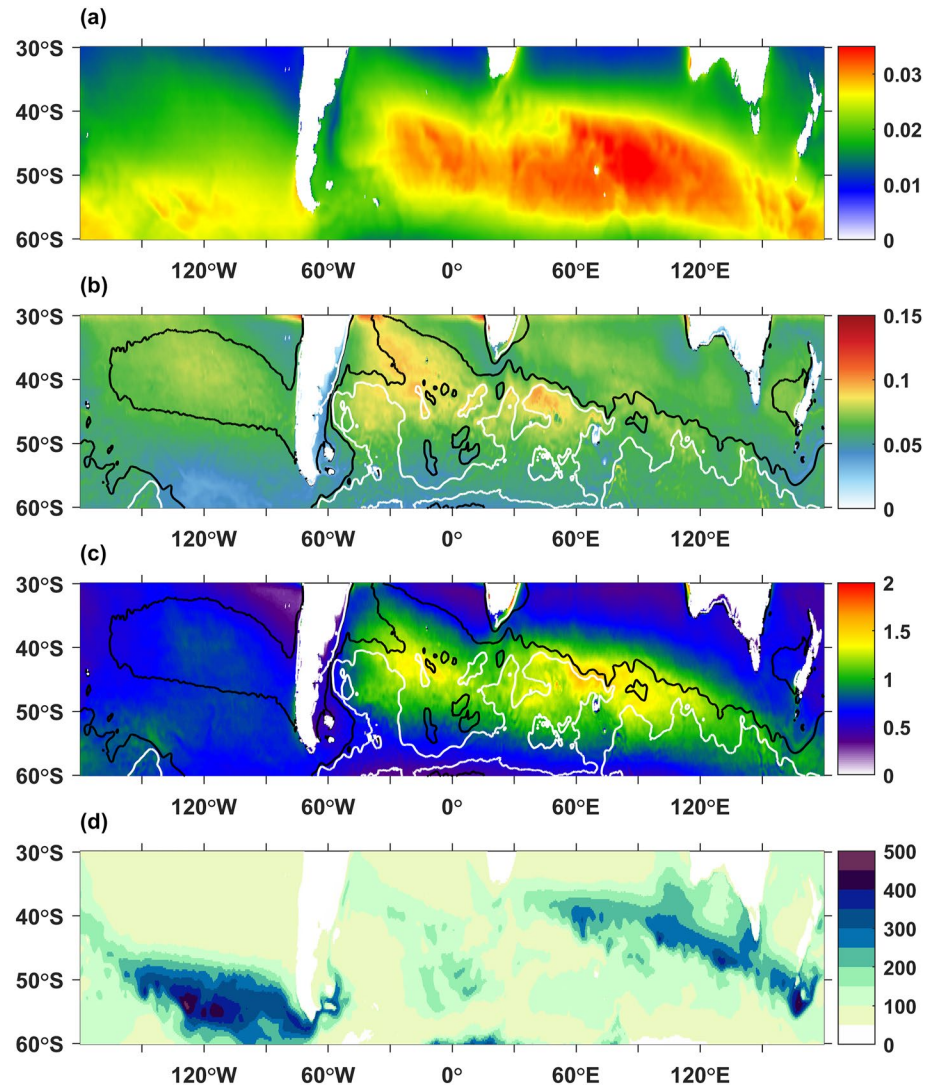
Figure 1. (a) NIWSM (N/m²), (b) the magnitude of surface near-inertial currents (m/s), (c) WPI$_i$ (mW/m²), and (d) MLD (m), averaged between 1979 and 2019. Black solid and white dashed represent $|\tau_i|/H$ contours of 0.0002 and 0.0003 N/m³, respectively.

proportional to the MLD (e.g., Pollard & Millard, 1970; D'Asaro, 1985; Rath et al., 2013, 2014; Zhai, 2015). As a result, regions with a large MLD, such as the area immediately to the south of Australia and to the west of South America (enclosed by the white solid contours), exhibit moderate to weak surface near-inertial currents, despite having relatively high levels of NIWSM (Figures 1b and 1d). Conversely, several regions with weak NIWSM but small MLD experience moderate levels of near-inertial currents. The combination of large NIWSM and small MLD results in a hot spot of near-inertial currents to the southwest of the Indian Ocean. Due to the overall decrease of the MLD northward of approximately 50°S, the peak of the zonal-mean $|u_i|$ is shifted nearly 10° toward the equator compared to that of the zonal-mean $|\tau_i|$ (Figure S1b in Supporting Information S1).

The spatial distribution of WPI$_i$ exhibits a pronounced zonal asymmetry, with elevated values in the South Atlantic, South Indian Ocean and to the south of Australia, while lower values are seen in the remainder of the South Pacific. The average value of WPI$_i$ in the South Atlantic (60°W–20°E), South Indian and to the south of Australia (20°E–140°E), and the remainder of the South Pacific (140°E–60°W) is about 0.81 mW/m², 0.85 mW/m² and 0.6 mW/m², respectively. The overall pattern of WPI$_i$ is consistent with that estimated from surface drifters and satellite wind measurements (Liu et al., 2019), although the maximum WPI$_i$ values in our model is somewhat smaller due to the weaker simulated near-inertial currents compared to the drifters. The average WPI$_i$ across
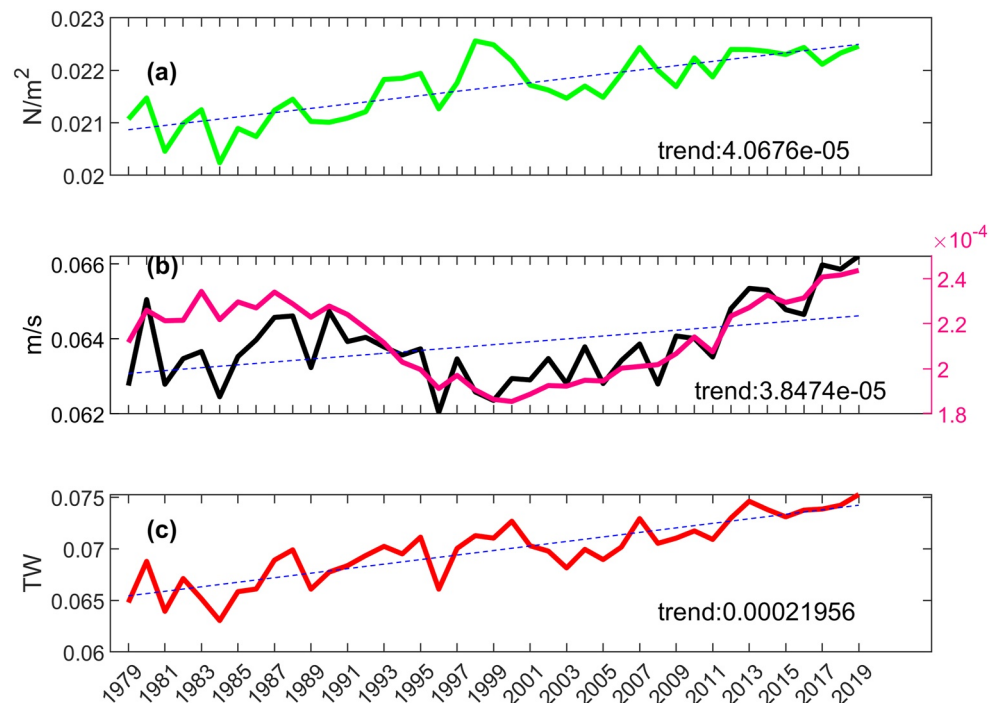
Figure 2. Time series and trend (blue dashed) of (a) NIWSM (N/m², green solid), (b) the magnitude of near-inertial surface currents (m/s, black solid) and the ratio of NIWSM to MLD (N/m³, magenta solid), and (c) WPI_i (mW/m², red solid) averaged between 30°S and 60°S and between 1979 and 2019. All trends are statistically significant at <1% level.

the entire model domain is about 0.07 TW which is greater than the 0.053 TW found by Rath et al. (2013) for the Southern Ocean (78°S–30°S) where they employed a coarser 6 hourly reanalysis wind product. The peak of the zonal-mean WPI_i falls between the peaks of the zonal-mean mean $|u_i|$ and zonal-mean $|\tau_i|$ and it is located approximately 5° equatorward of the peak of the zonal-mean $|\tau_i|$ (Figure S1 in Supporting Information S1).

3.2. Trends

In this section we analyze the trends of NIWSM, surface near-inertial currents, and WPI_i averaged over the Southern Ocean. All trends are statistically significant at <1% level by *t*-test.

During the 41-year study period, the domain-averaged NIWSM in the Southern Ocean has shown a significant increase, with a positive trend of approximately 4.1×10^{-5} N/m²/yr (Figure 2a). In comparison, the annual mean wind stress exhibits a higher increasing trend of 1.6×10^{-4} N/m²/yr, which is about four times of the NIWSM trend (Figure S2 in Supporting Information S1). The strengthening of near-inertial wind forcing in the Southern Ocean in recent decades has also been reported by Rath et al. (2014) based on analysis of a 6 hourly wind reanalysis product. The average magnitude of surface near-inertial currents, on the other hand, is found to decrease slightly during the first half of the study period which is followed by a rapid increase, resulting in an overall upward trend of 3.8×10^{-5} m/s/yr over the entire 41-year period (Figure 2b). To address the discrepancy between the trends of NIWSM and the magnitude of near-inertial currents, we consider the changes in MLD by plotting the time series of domain-averaged $|\tau_i|/H$. The close correspondence between the time series of $|\tau_i|/H$ and $|u_i|$ highlights the importance of MLD changes in modulating the trend of surface near-inertial currents.

WPI_i in the Southern Ocean increases by about 17% over the 1979–2019 period, with a positive trend of 2.2×10^{-4} TW per year (Figure 2c). The domain-integrated WPI_i varies from 64 GW in 1984 to 75 GW in 2019. Although the general trends of WPI_i and NIWSM appear similar, they do not consistently align with each other on a year-to-year basis. For example, the strongest NIWSM in 1998 does not correspond to the largest WPI_i. This discrepancy can be attributed to the deep surface mixed layer in 1998 (Figure S2 in Supporting Information S1) which results in a smaller $|\tau_i|/H$ and consequently weaker surface near-inertial currents (Figure 2b).
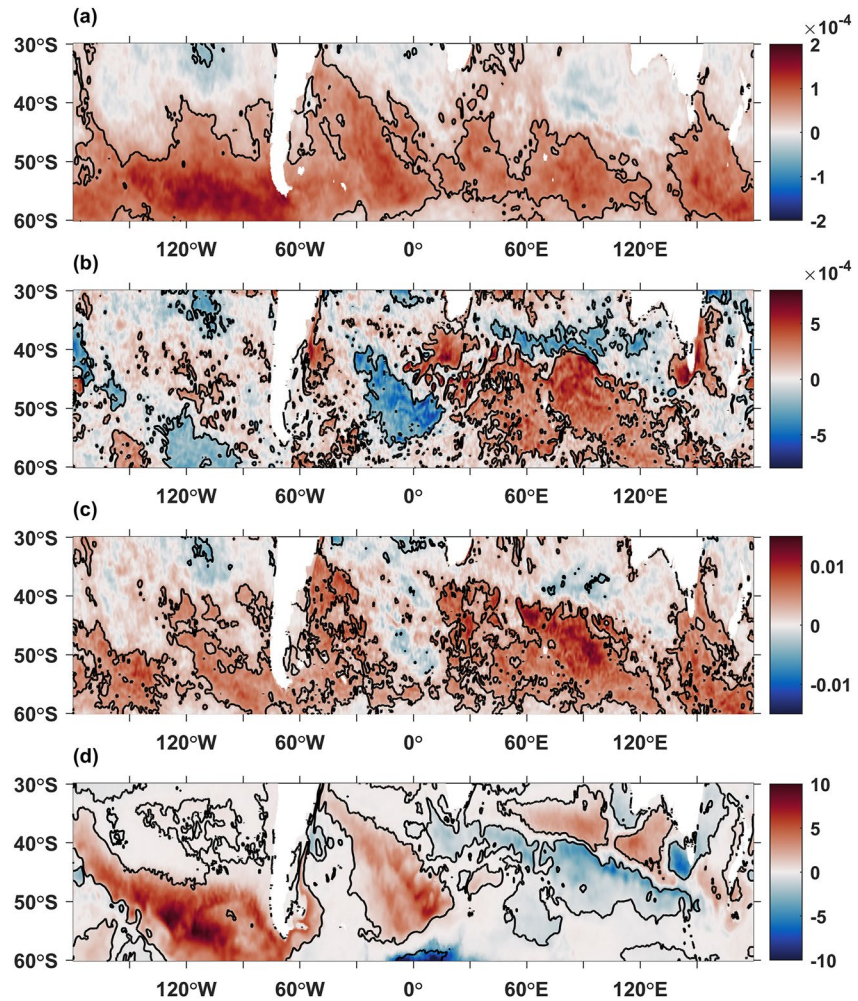
Figure 3. The trends of (a) NIWSM (N/m^2), (b) the magnitude of near-inertial surface currents (m/s), (c) WPI$_i$ (mW/m^2), and (d) MLD (m) during 1979–2019. Black solid contours mark the 95% confidence level.

Figure 3a shows that the positive trend of NIWSM is broadly distributed, with large values mostly concentrated in the latitude band of 40°–60°S. The highest trend of NIWSM is found in the eastern South Pacific. In contrast, the surface near-inertial currents exhibit a mixture of positive and negative trends (Figure 3b). There are three regions where the trend of $|u_i|$ is significantly negative, including the eastern South Pacific. This discrepancy between the trends of NIWSM and $|u_i|$ can be explained by the zonally asymmetric changes of MLD in response to air-sea heat flux anomalies associated with the Southern Annular Mode (Figure S3 in Supporting Information S1; Sallee et al., 2010). Over the study period, these three regions with a negative $|u_i|$ trend have experienced a significant deepening of the surface mixed layer (Figure 3d), which results in weaker $|u_i|$ despite the strengthening trend of NIWSM in those areas. As a result, the trend of WPI$_i$ appears more patchy (Figure 3c), and the most significant positive trend of WPI$_i$ is found in the Indian Ocean south of 40°S, where NIWSM has increased and the mixed layer has become shallower. Rath et al. (2014) estimated the trend of WPI$_i$ in recent decades based on the analysis of NIWSM alone, neglecting changes in MLD. Our study demonstrates the role of MLD in modulating the spatial pattern and trend of WPI$_i$ and highlights the limitations of predicting future changes in near-inertial motions and associated mixing using atmospheric forcing alone.

To assess whether the trend in NIWSM is due to changes in mesoscale or synoptic weather systems, we analyze eddy kinetic energy associated with wind fluctuations on time scales of 1 h–2 days (EKE$_{<2d}$) and 2–8 days (EKE$_{2-8d}$). Following Lin et al. (2018), EKE$_{<2d}$ is calculated using the difference between the hourly and 2-day running mean wind fields and EKE$_{2-8d}$ is calculated using the difference between the 2-day running mean and 8-day running mean wind fields.
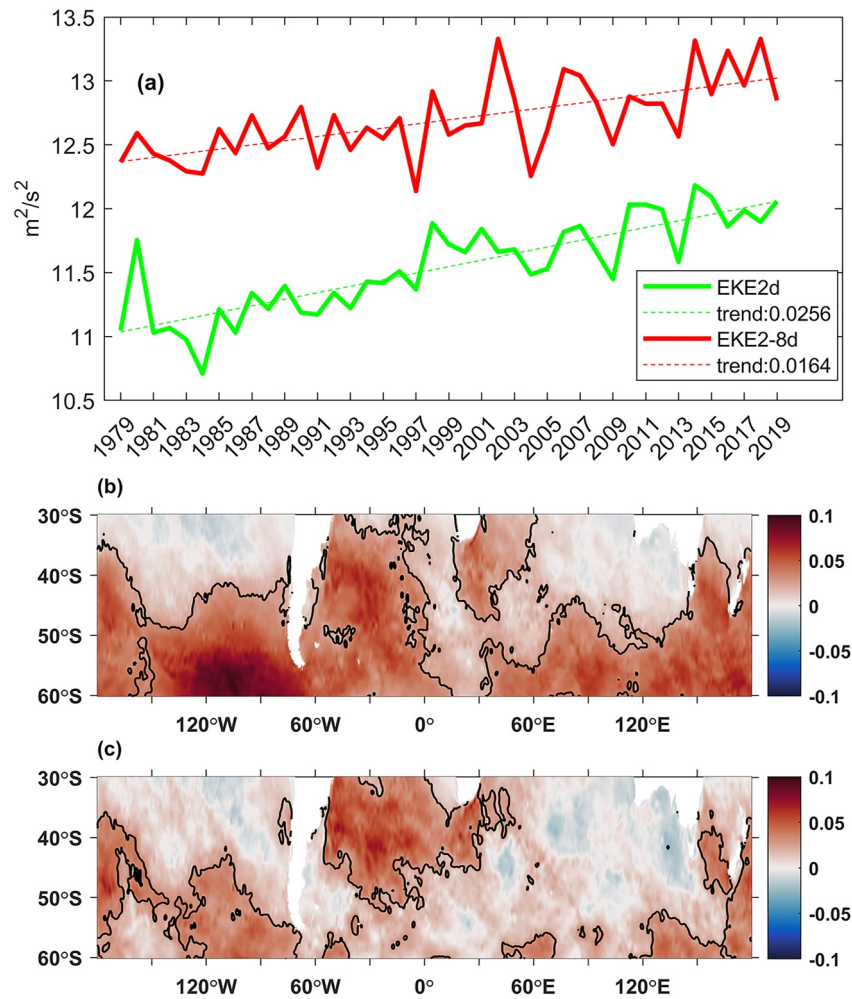
Figure 4. (a) Time series of kinetic energy associated with mesoscale and synoptic weather systems. (b) Spatial distribution of kinetic energy trend associated with mesoscale weather systems during 1979–2019. Panel (c) same as (b) but for synoptic weather systems. Black solid contours in (b) and (c) mark the 95% confidence level.

Both mesoscale and synoptic weather systems exhibit significant increasing trends over the 1979–2019 period. Notably, the trend of $EKE_{<2d}$ exceeds that of EKE_{2-8d} by more than 50% (Figure 4a). This result is consistent with the study of Lin et al. (2018) who analyzed three atmospheric reanalysis products of lower resolution and reported a greater strengthening trend of mesoscale weather systems than synoptic systems in the Southern Ocean during recent decades. Furthermore, compared to EKE_{2-8d}, the spatial distribution of the trend of $EKE_{<2d}$ corresponds more closely to that of NIWSM (Figures 4b and 4c). For example, both $EKE_{<2d}$ and NIWSM display extensive positive trends within the latitude range of 40–60°S, and both have their peak positive trends situated in the South Pacific Ocean. The significant positive trend of $EKE_{<2d}$ in the South Pacific aligns with the observed increase in mesoscale cyclone frequency over the Amundsen and Bellingshausen Seas (Irving et al., 2010). This increase in mesoscale cyclone frequency is thought to be related to the concurrent positive trend of the Southern Annular Mode over recent decades (Irving et al., 2010; Rath et al., 2014). Our results thus suggest that changes in mesoscale weather systems are the main driver behind the positive trend of NIWSM over the 41-year study period.

4. Conclusions

In this study, we have examined the spatial pattern and trend of wind power input to near-inertial motions in the Southern Ocean from 1979 to 2019 using a global eddy-permitting OGCM forced by hourly ERA5 atmospheric reanalysis data. The spatial distribution of WPI_i is found to exhibit a pronounced zonal asymmetry, with elevated

values in the South Atlantic and South Indian Ocean, while lower values are seen in the South Pacific, particularly to the southwest of Australia. WPI_i integrated between 30°S and 60°S shows a significant positive trend during the 41-year study period. Our results suggest that this positive trend of WPI_i is largely attributed to the increasing near-inertial wind stress associated with the intensification of mesoscale weather systems. Our result also highlights the role of the surface mixed-layer depth in modulating the distribution and trend of WPI_i by altering the magnitude of surface near-inertial currents.

Recent studies based on convection-permitting atmospheric simulations (e.g., Chan et al., 2023; Schumacher & Rasmussen, 2020) predict changes in the intensity and frequency of mesoscale weather systems under a warming climate. The future warming of the Southern Ocean (e.g., Cai et al., 2010) may create more favorable conditions for the generation of mesoscale cyclones. It remains an open question whether the upward trend of WPI_i found in this study will continue into the next decade. Further research is also required to investigate the consequences of this significant increase in WPI_i on ocean mixing and circulation.

Data Availability Statement

ERA5 data were obtained from the European Centre for Medium-Range Weather Forecasts (https://cds.climate.copernicus.eu/cdsapp#!/dataset/reanalysis-era5-single-levels?tab=overview). The MITgcm code was obtained freely from http://mitgcm.org/. Our model data, configuration and input directories can be downloaded at https://doi.org/10.5281/zenodo.8298366.

References

Adcroft, A., Campin, J.-M., Hill, C., & Marshall, J. (2004). Implementation of an atmosphere–ocean general circulation model on the expanded spherical cube. *Monthly Weather Review*, *132*(12), 2845–2863. https://doi.org/10.1175/MWR2823.1

Alford, M. H. (2001). Internal swell generation: The spatial distribution of energy flux from the wind to mixed layer near-inertial motions. *Journal of Physical Oceanography*, *31*(8), 2359–2368. https://doi.org/10.1175/1520-0485(2001)031<2359:ISGTSD>2.0.CO;2

Alford, M. H. (2003). Improved global maps and 54-year history of wind-work on ocean inertial motions. *Geophysical Research Letters*, *30*(8). https://doi.org/10.1029/2002GL016614

Cai, W., Cowan, T., Godfrey, S., & Wijffels, S. (2010). Simulations of processes associated with the fast warming rate of the southern midlatitude ocean. *Journal of Climate*, *23*(1), 197–206. https://doi.org/10.1175/2009JCLI3081.1

Chaigneau, A., Pizarro, O., & Rojas, W. (2008). Global climatology of near-inertial current characteristics from Lagrangian observations. *Geophysical Research Letters*, *35*(13), L13603. https://doi.org/10.1029/2008GL034060

Chan, S. C., Kendon, E. J., Fowler, H. J., Kahraman, A., Crook, J., Ban, N., & Prein, A. F. (2023). Large-scale dynamics moderate impact-relevant changes to organised convective storms. *Communications Earth & Environment*, *4*(1), 8. https://doi.org/10.1038/s43247-022-00669-2

Chang, E. K., Guo, Y., & Xia, X. (2012). CMIP5 multimodel ensemble projection of storm track change under global warming. *Journal of Geophysical Research*, *117*(D23). https://doi.org/10.1029/2012JD018578

Chemke, R., Ming, Y., & Yuval, J. (2022). The intensification of winter mid-latitude storm tracks in the Southern Hemisphere. *Nature Climate Change*, *12*(6), 553–557. https://doi.org/10.1038/s41558-022-01368-8

Copernicus Climate Change Service (C3S). (2017). ERA5: Fifth generation of ECMWF atmospheric reanalyses of the global climate. *Copernicus Climate Change Service Climate Data Store (CDS)*. Retrieved from https://cds.climate.copernicus.eu

Crawford, G., & Large, W. (1996). A numerical investigation of resonant inertial response of the ocean to wind forcing. *Journal of Physical Oceanography*, *26*(6), 873–891. https://doi.org/10.1175/1520-0485(1996)026<0873:ANIORI>2.0.CO;2

D'Asaro, E. A. (1985). The energy flux from the wind to near-inertial motions in the surface mixed layer. *Journal of Physical Oceanography*, *15*(8), 1043–1059. https://doi.org/10.1175/1520-0485(1985)015<1043:TEFFTW>2.0.CO;2

Dippe, T., Zhai, X., Greatbatch, R. J., & Rath, W. (2015). Interannual variability of wind power input to near-inertial motions in the North Atlantic. *Ocean Dynamics*, *65*(6), 859–875. https://doi.org/10.1007/s10236-015-0834-x

Elipot, S., & Lumpkin, R. (2008). Spectral description of oceanic near-surface variability. *Geophysical Research Letters*, *35*(5), L05606. https://doi.org/10.1029/2007GL032874

Flexas, M. M., Thompson, A. F., Torres, H. S., Klein, P., Farrar, J. T., Zhang, H., & Menemenlis, D. (2019). Global estimates of the energy transfer from the wind to the ocean, with emphasis on near-inertial oscillations. *Journal of Geophysical Research: Oceans*, *124*(8), 5723–5746. https://doi.org/10.1029/2018JC014453

Furuichi, N., Hibiya, T., & Niwa, Y. (2008). Model-predicted distribution of wind-induced internal wave energy in the world's oceans. *Journal of Geophysical Research*, *113*(C9), C09034. https://doi.org/10.1029/2008JC004768

Holte, J., Talley, L. D., Gilson, J., & Roemmich, D. (2017). An Argo mixed layer climatology and database. *Geophysical Research Letters*, *44*(11), 5618–5626. https://doi.org/10.1002/2017GL073426

Irving, D., Simmonds, I., & Keay, K. (2010). Mesoscale cyclone activity over the ice-free Southern Ocean: 1999-2008. *Journal of Climate*, *23*(20), 5404–5420. https://doi.org/10.1175/2010JCLI3628.1

Jiang, J., Lu, Y., & Perrie, W. (2005). Estimating the energy flux from the wind to ocean inertial motions: The sensitivity to surface wind fields. *Geophysical Research Letters*, *32*(15), L15610. https://doi.org/10.1029/2005GL023289

Jochum, M., Briegleb, B. P., Danabasoglu, G., Large, W. G., Norton, N. J., Jayne, S. R., et al. (2013). The impact of oceanic near-inertial waves on climate. *Journal of Climate*, *26*(9), 2833–2844. https://doi.org/10.1175/JCLI-D-12-00181.1

Kara, A. B., Rochford, P. A., & Hurlburt, H. E. (2000). An optimal definition for ocean mixed layer depth. *Journal of Geophysical Research*, *105*(C7), 16803–16821. https://doi.org/10.1029/2000JC900072

Kunze, E. (1985). Near-inertial wave propagation in geostrophic shear. *Journal of Physical Oceanography*, *15*(5), 544–565. https://doi.org/10.1175/1520-0485(1985)015<0544:NIWPIG>2.0.CO;2

Large, W., & Pond, S. (1981). Open ocean momentum flux measurements in moderate to strong winds. *Journal of Physical Oceanography*, *11*(3), 324–336. https://doi.org/10.1175/1520-0485(1981)011<0324:OOMFMI>2.0.CO;2

Large, W. G., McWilliams, J. C., & Doney, S. C. (1994). Oceanic vertical mixing: A review and a model with a nonlocal boundary layer parameterization. *Reviews of Geophysics*, *32*(4), 363–403. https://doi.org/10.1029/94RG01872

Lin, X., Zhai, X., Wang, Z., & Munday, D. R. (2018). Mean, variability, and trend of Southern Ocean wind stress: Role of wind fluctuations. *Journal of Climate*, *31*(9), 3557–3573. https://doi.org/10.1175/JCLI-D-17-0481.1

Liu, Y., Jing, Z., & Wu, L. (2019). Wind power on oceanic near-inertial oscillations in the global ocean estimated from surface drifters. *Geophysical Research Letters*, *46*(5), 2647–2653. https://doi.org/10.1029/2018GL081712

Marshall, J., Adcroft, A., Hill, C., Perelman, L., & Heisey, C. (1997). A finite-volume, incompressible Navier Stokes model for studies of the ocean on parallel computers. *Journal of Geophysical Research*, *102*(C3), 5753–5766. https://doi.org/10.1029/96JC02775

Marshall, J., Hill, C., Perelman, L., & Adcroft, A. (1997). Hydrostatic, quasi-hydrostatic, and nonhydrostatic ocean modeling. *Journal of Geophysical Research*, *102*(C3), 5733–5752. https://doi.org/10.1029/96JC02776

McPhee, M. G. (1980). An analysis of pack ice drift in summer. In R. S. Pritchard (Ed.), *Sea-ice processes and models* (pp. 62–75). Univ. of Wash. Press.

Menemenlis, D., Hill, C., Adcrocft, A., Campin, J. M., Cheng, B., Ciotti, B., et al. (2005). NASA supercomputer improves prospects for ocean climate research. *Eos, Transactions American Geophysical Union*, *86*(9), 89–96. https://doi.org/10.1029/2005EO090002

Pezza, A., Sadler, K., Uotila, P., Vihma, T., Mesquita, M. D., & Reid, P. (2016). Southern Hemisphere strong polar mesoscale cyclones in high-resolution datasets. *Climate Dynamics*, *47*(5–6), 1647–1660. https://doi.org/10.1007/s00382-015-2925-2

Plueddemann, A., & Farrar, J. (2006). Observations and models of the energy flux from the wind to mixed-layer inertial currents. *Deep Sea Research Part II: Topical Studies in Oceanography*, *53*(1–2), 5–30. https://doi.org/10.1016/j.dsr2.2005.10.017

Pollard, R. T., & Millard, R., Jr. (1970). Comparison between observed and simulated wind-generated inertial oscillations. In *Paper presented at the deep sea research and oceanographic abstracts*. https://doi.org/10.1016/0011-7471(70)90043-4

Rasmussen, E. A., & Turner, J. (2003). *Polar lows: Mesoscale weather systems in the polar regions* (p. 612). Cambridge University Press.

Rath, W., Greatbatch, R. J., & Zhai, X. (2013). Reduction of near-inertial energy through the dependence of wind stress on the ocean-surface velocity. *Journal of Geophysical Research: Oceans*, *118*(6), 2761–2773. https://doi.org/10.1002/jgrc.20198

Rath, W., Greatbatch, R. J., & Zhai, X. (2014). On the spatial and temporal distribution of near-inertial energy in the Southern Ocean. *Journal of Geophysical Research: Oceans*, *119*(1), 359–376. https://doi.org/10.1002/2013JC009246

Rimac, A., von Storch, J. S., Eden, C., & Haak, H. (2013). The influence of high-resolution wind stress field on the power input to near-inertial motions in the ocean. *Geophysical Research Letters*, *40*(18), 4882–4886. https://doi.org/10.1002/grl.50929

Sallée, J.-B., Speer, K., & Rintoul, S. (2010). Zonally asymmetric response of the Southern Ocean mixed-layer depth to the Southern Annular Mode. *Nature Geoscience*, *3*(4), 273–279. https://doi.org/10.1038/ngeo812

Schumacher, R. S., & Rasmussen, K. L. (2020). The formation, character and changing nature of mesoscale convective systems. *Nature Reviews Earth & Environment*, *1*(6), 300–314. https://doi.org/10.1038/s43017-020-0057-7

Simmons, H. L., & Alford, M. H. (2012). Simulating the long-range swell of internal waves generated by ocean storms. *Oceanography*, *25*(2), 30–41. https://doi.org/10.5670/oceanog.2012.39

Uotila, P., Pezza, A. B., Cassano, J. J., Keay, K., & Lynch, A. H. (2009). A comparison of low pressure system statistics derived from a high-resolution NWP output and three reanalysis products over the Southern Ocean. *Journal of Geophysical Research*, *114*(D17), D17105. https://doi.org/10.1029/2008JD011583

Verezemskaya, P., Tilinina, N., Gulev, S., Renfrew, I. A., & Lazzara, M. (2017). Southern Ocean mesocyclones and polar lows from manually tracked satellite mosaics. *Geophysical Research Letters*, *44*(15), 7985–7993. https://doi.org/10.1002/2017GL074053

Watanabe, M., & Hibiya, T. (2002). Global estimates of the wind-induced energy flux to inertial motions in the surface mixed layer. *Geophysical Research Letters*, *29*(8), 64-61–64-63. https://doi.org/10.1029/2001GL014422

Wunsch, C., & Ferrari, R. (2004). Vertical mixing, energy, and the general circulation of the oceans. *Annual Review of Fluid Mechanics*, *36*(1), 281–314. https://doi.org/10.1146/annurev.fluid.36.050802.122121

Yin, J. H. (2005). A consistent poleward shift of the storm tracks in simulations of 21st century climate. *Geophysical Research Letters*, *32*(18). https://doi.org/10.1029/2005GL023684

Zhai, X. (2015). Latitudinal dependence of wind-induced near-inertial energy. *Journal of Physical Oceanography*, *45*(12), 3025–3032. https://doi.org/10.1175/JPO-D-15-0166.1

Zhai, X. (2017). Dependence of energy flux from the wind to surface inertial currents on the scale of atmospheric motions. *Journal of Physical Oceanography*, *47*(11), 2711–2719. https://doi.org/10.1175/JPO-D-17-0073.1